Numerical Study on Hydrodynamics Analysis of Geldart B Group of Particles in a 2D Fluidized Bed Drier

Vasujeet Singh, Pruthiviraj Nemalipuri, Vivek Vitankar, Harish Chandra Das, Malay Kumar Prdhan, and Swaroop Jena

Abstract Bubbling fluidized bed boilers are the most extensive fluidized bed application in chemical industries—the CFD simulation of non-reactive two-dimensional fluidized bed drier has been carried out using the Eulerian–Eulerian two-fluid method with Geldart B group of particles, using Fluent 2020R2 software. A comparative study at three different sizes of particles (0.180, 0.280 and 0.380 mm) using Syamlal O'brien drag models for a wide range of velocity (0.1–1 m/s) has been performed. $k - \varepsilon$ turbulence model has been used to model the turbulence and mixing inside the system. CFD. The model is validated with the existing experimental data and shows good agreement. Numerical results show that fluidized bed pressure drops increased as particle diameter increased, and further, the value of bed pressure drop increases as the superficial gas velocity increases up to the minimum fluidization velocity (0.184 m/s), beyond which there is no additional rise in bed pressure drop as the superficial gas velocity increases. It has also been noticed that disperse phase particles form clusters near the riser's wall due to its shear effects.

Keywords CFD · CFBC · Boiler · Bed material

V. Singh · P. Nemalipuri (✉) · H. C. Das
Department of Mechanical Engineering, National Institute of Technology Meghalaya, Shillong, India
e-mail: pruthiviraj@nitm.ac.in

V. Vitankar
FluiDimensions, Pune, India

M. K. Prdhan
Government of Odisha, OSDMA, Bhubaneswar, India

S. Jena
Factories and Boilers, Government of Odisha, Bhubaneswar, India

P. Pradhan et al. (eds.), *Recent Advances in Mechanical Engineering*,
Lecture Notes in Mechanical Engineering,
https://doi.org/10.1007/978-981-16-9057-0_71

Abbreviations

α_l	Fluid Phase Volume Fraction
ρ_l	Density of Fluid
v_l	Velocity of Fluid
α_s	Dispersed Phase Volume Fraction
ρ_s	Density of Dispersed Phase
v_s	Velocity of Dispersed Phase
θ_s	Granular Temperature
e_{ss}	Restitution Coefficient
ε_s	Bulk Viscosity
T_s	Particle Relaxation Time
Re_s	Reynolds Number
γ_{θ_s}	Collisional Dissipation
ρ_{sus}	Suspension Density
g_o	Radial Particle Distribution Function
P_s	Solid Pressure
$\emptyset$	Internal Frictional Angle
I_{2D}	Second Invariant of Devitorial Stress Tensor
θ_s	Granular Temperature
e_{ss}	Restitution Coefficient
τ_l	Stress Tensor for Fluid Phase
τ_s	Stress Tensor for Dispersed Phase
K_{sl}	Fluid–Solid Exchange Coefficient
C_d	Drag Coefficient
k_{θ_s}	Diffusion Coefficient
Δh	Difference in Water Column

1 Introduction

Fluidized bed driers are most widely used in the pharmaceutical and agriculture industries. Fluidization is used for the process to obtain quality grains from the paddy with minimum damage to pests [1, 2]. A comprehensive simulation study on different internment heat pump drying for moisture diffusion, energy consumption and drying time on Chinese cabbage seeds was carried out by Ebert et al. [3]. The results indicate that in intermediate drying percentage of energy-saving was 48.1% over continuous drying. The hydrodynamics and heat transfer characteristics at four different % (2.5%, 7.5%, 12.5% and 20%) mixing of biomass and sand in a pressurized circulating fluidized bed have been investigated by Kalita et al. [4, 5] at a superficial gas velocity of 6, 7, 8 m/s and system pressure of 1, 3 and 5 bar. They reported that higher pressure and higher superficial gas velocity are found favourable

for achieving a higher heat transfer coefficient. Biomass blending of 12.5% and a pressure of 5 bar are optimum to achieve a maximum wall to bed heat transfer coefficient and uniform circulation rate. Another industrial application of fluidization is fluidized bed boiler which comes into the picture in 1960s. In only two decades, it becomes the workhorse of 40–50% of power production industries due to its numerous advantages over conventional furnaces [6, 7]. In chemical industries, most of the problems are multiphase and multiphysics. More than one physical phenomenon is intermingling together, so the mathematical modelling of such problems is not straightforward [8, 9]. Two distinct approaches (Eulerian–Eulerian and Eulerian–Lagrangian) have been used to solve the multiphase flow problems. In the Eulerian–Eulerian approach, both the phases (fluid phase and dispersed particle phase) are considered as an interpenetrating continuum. In this approach, both fluid and dispersed particulate phases are being solved using a separate set of conservation equations. From the experimentation, it has been concluded that the Eulerian–Eulerian approach is suitable for high dispersed phase volume fraction (>20%) [10–12]. The second approach is Eulerian–Lagrangian approach. The fluid phase is solved using conservation equations, and the dispersed particulate phase is solved using Newtonian mechanics [13, 14]. Experiments suggest that this approach is more accurate as compared to the Eulerian–Eulerian approach and suitable for low dispersed phase volume fraction (<20%) [15]. Fluidized bed boilers have a high (<40%) solid volume fraction, so the current research problem also has been solved using the Eulerian–Eulerian approach. Kinetic theory of granular flow also has been incorporated to solve the dispersed phase collisions. Bubble formation, variation in the flow patterns, bed voidage and other hydrodynamics parameters are investigated for three different particle diameters at different gas velocity. In this current research hydrodynamic study of a 2D fluidized bed, riser has been carried out. The effect of superficial gas velocity on bed pressure drop, void fraction and solid volume fraction has been analysed for three different particle diameters (0.180, 0.280, 0.380 mm).

2 Computational Modelling and Boundary Conditions

CFD Simulations were performed to understand hydrodynamics in a CFB drier. The Eulerian–Eulerian multiphase model was applied to solve the multiphase flow physics of gas and granular phase. The Eulerian–Eulerian theory states that gas and dispersed phases are mathematically interpenetrating continua with each other. The kinetic theory of granular flow, which conserves the energy associated with random particle fluctuation, has been used to close solid stress terms in multiphase flow equations. The standard $k - \varepsilon$ turbulence model is used to simulate the mixing and turbulence generated inside the system. Unsteady-state simulation with a time step size of 0.001 s and 50 iterations per time step is done on a two-dimensional computational domain discretized into square cells. The governing equations are solved using the SIMPLE algorithm with a second-order discretization scheme (Table 1; Fig. 1).

Table 1 Mathematical modelling parameters

S. No.	Modelling parameters	Value
1	Riser height	1000 mm
2	Riser width	280 mm
3	Mean particle diameter	180 μm, 280 μm, 380 μm
4	Particle density	4200 kg/m^3
5	Gas density	1.225 kg/m^3
6	Gas viscosity	1.8×10^{-5} kg/m-s
7	Static bed height	300 mm
8	Minimum fluidization velocity	0.1179 m/s
9	Superficial gas velocity	0.1–1 m/s
1	Restitution coefficient	0.9
2	Solid volume fraction	0.55
3	X mesh spacing	5 mm
4	Y mesh spacing	5 mm
5	Number of elements	8960
6	Number of nodes	9177
7	Multiphase model	Eulerian–Eulerian
8	Drag model	Syamlal O'brien
9	Time step size	0.001 s
10	Number of time step	8000
11	Maximum iteration per time step	50

3 Conservation of Mass Equations for Fluid and Dispersed Phase

$$\frac{\partial(\alpha_l \rho_l)}{\partial t} + \nabla(\alpha_l \rho_l v_l) = 0 \tag{1}$$

$$\frac{\partial(\alpha_s \rho_s)}{\partial t} + \nabla(\alpha_s \rho_s v_s) = 0 \tag{2}$$

The following is the Navier–Stokes equation for the gas phase and the particulate phase:

$$\frac{\partial(\alpha_l \rho_l v_l)}{\partial t} + \nabla(\alpha_l \rho_l v_l v_l) = -\alpha_l \nabla P + \nabla \tau_l + \alpha_l \rho_l \vec{g} + F_{\text{ext}} \tag{3}$$

$$\frac{\partial(\alpha_s \rho_s v_s)}{\partial t} + \Delta(\alpha_s \rho_s v_s v_s) = -\alpha_s \Delta P - \nabla P_s + \Delta \overrightarrow{\tau_s} + \alpha_s \rho_s \vec{g} + F_{\text{ext}} \tag{4}$$

In the Eulerian–Eulerian model, solid pressure is given below,

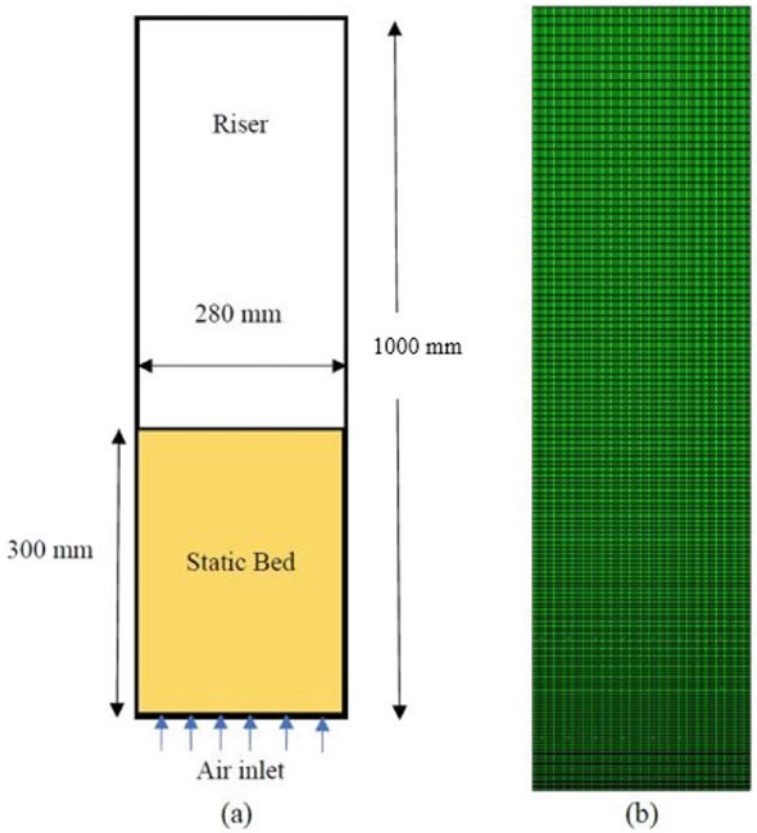

Fig. 1 **a** Dimension of setup. **b** Quadrilateral mesh used for simulation

$$P_s = \alpha_s \rho_s \theta_s + 2\rho_s(1 + e_{ss})\alpha_s^2 g_o \theta_s \tag{5}$$

$$g_o = \left[1 - \left(\frac{\alpha_s}{\alpha_{s_{\max}}}\right)^{1/3}\right]^{-1} \tag{6}$$

Solid viscosity is defined as the sum of viscosity due to collision with other particles, viscosity due to the fluctuation in kinetic energy and viscosity due to friction.

$$\mu_{\text{Solid}} = \mu_{\text{Collisional}} + \mu_{\text{kin}} + \mu_{\text{friction}} \tag{7}$$

4 Collisional Viscosity

$$\mu_{\text{Col}} = \frac{4}{5}\alpha_s \rho_s d_s g_o (1 + e_{ss}) \left(\frac{\theta_s}{\pi}\right)^{1/2} \tag{8}$$

5 Viscosity Due to Fluctuation in Kinetic Energy

$$\mu_{\text{kin}} = \frac{\alpha_s d_s \rho_s \sqrt{\theta_s \pi}}{6(3 - e_{ss})} \left[1 + \frac{2}{5}(1 + e_{ss})(3e_{ss} - 1)\alpha_s g_o\right] \tag{9}$$

6 Frictional Viscosity

$$\mu_f = \frac{P_s \sin \emptyset}{2\sqrt{I_{2D}}} \tag{10}$$

In Navier–Stokes equation, τ_l and τ_s represent the stress tensor for the gas phase and the solid phase, respectively.

$$\tau_l = \alpha_l \mu_l \left(\nabla \vec{v}_l + \nabla \vec{v}_l^t\right) - \frac{2}{3}\alpha_l \mu_l (\nabla . \vec{v}_l) \overline{\overline{I}}_l \tag{11}$$

$$\tau_s = \alpha_s \mu_s \left(\nabla \vec{v}_s + \nabla \vec{v}_s^t\right) - \alpha_s \left(\varepsilon_s - \frac{2}{3}\mu_s\right) . \vec{v}_s \tag{12}$$

In Eq. (10), ε_s is the bulk viscosity and it uses to calculate the expansion and depression resistance of the particles given by Lun et al.

$$\varepsilon_s = \frac{4}{3}\alpha_s d_s \rho_s g_o (1 + e) \left(\frac{\theta_s}{\pi}\right)^{1/2} \tag{13}$$

Syamlal O'brien drag model has been used to simulate the drag force over the particles, Fluid–solid exchange coefficient (K_{sl}) can be written in the following general form.

$$K_{sl} = \frac{\alpha_s \rho_s f}{T_s} \tag{14}$$

Fluid–solid exchange coefficients define by various researchers differently for different types of flow conditions. Drag factor, according to the Syamlal O'brien drag model, is defined as:

$$f = \frac{C_d \mathrm{Re}_s \alpha_l}{24 v_{rs}^2} \tag{15}$$

where C_d is the drag coefficient,

$$C_d = \left(0.63 + \frac{4.8}{\sqrt{R_{es}/v_{rs}}}\right)^2 \tag{16}$$

By putting the value of drag factor and the particle relaxation time, K_{sl} has the following form,

$$K_{sl} = \frac{3\alpha_s \alpha_l \rho_l}{4 v_{rs}^2 d_s} C_d \left(\frac{R_{es}}{v_{rs}}\right)(v_s - v_f) \tag{17}$$

V_{rs} stands for relative settling velocity, which is defined as the ratio of the particle's terminal settling velocity to the sphere's terminal settling velocity.

Where V_{rs} is the terminal velocity,

$$v_{rs} = 0.5\left(A - 0.06\mathrm{Re}_s + \sqrt{(0.06\mathrm{Re}_s)^2 + 0.12 R_{es}(2B - A) + A^2}\right) \tag{18}$$

$A = \alpha_l^{4.14}$
$B = 0.8\alpha_l^{1.28}$ for $\alpha_l < 0.85$
$B = \alpha_l^{2.65}$ for $\alpha_l > 0.85$.

7 Result and Discussions

To validate the mathematical model, results of bed pressure drop and bed density have been capered with the existing results of Zhao et al. [16]. Simulation results are in good agreement with the results of Zhao et al. [16] as depicted in Figs. 2, 3 and 4.

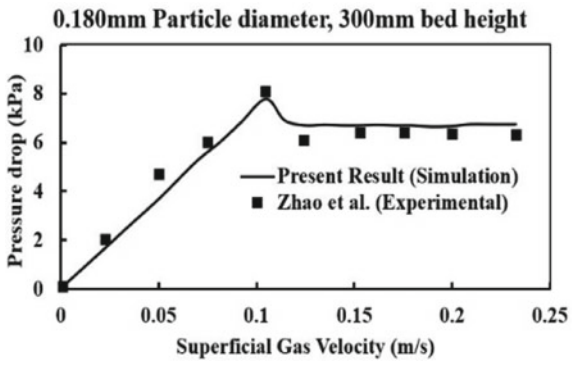

Fig. 2 Variation of bed pressure drop with superficial gas velocity

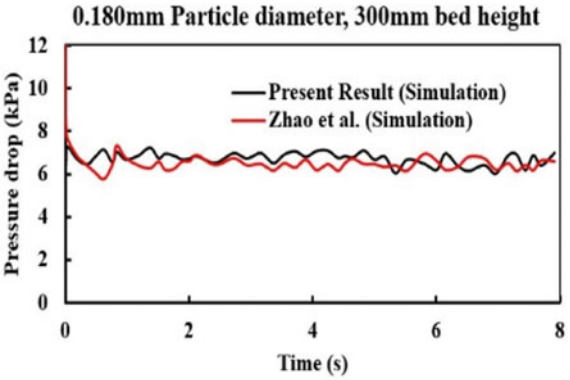

Fig. 3 Variation of bed pressure drop with time

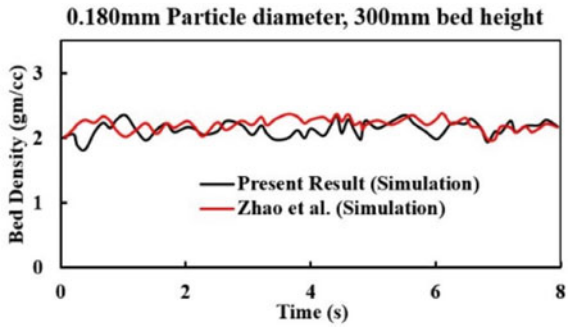

Fig. 4 Variation of bed density with time

Bed pressure drop has been measured at three different locations (100 mm, 350 mm and 600 mm) along with the height of the riser above the distributor plate. These points have been marked as P1, P2 and P3, respectively. By measuring the pressure drop at three different locations, this method helps in comparison with the lower and upper regions of bed pressure drop. Figure 5 shows the variation of bed pressure drop (P1–P3) with simulation time on the *X*-axis for three different sizes

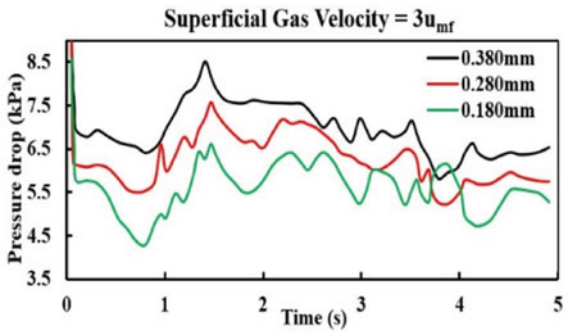

Fig. 5 Pressure drops (P1–P3) for different sizes of particles

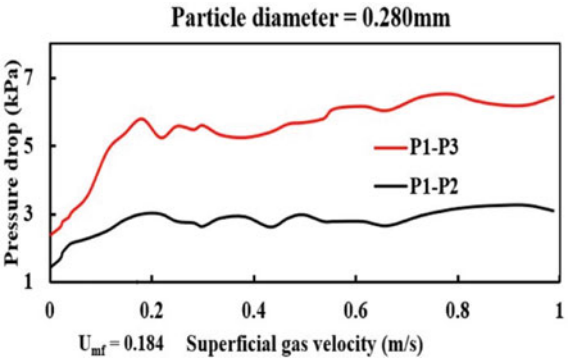

Fig. 6 Variation of pressure drop with superficial gas velocity

of particles (0.180, 0.280 and 0.380 mm). It can be concluded from Fig. 5 that more fluctuation in bed pressure drop has been observed up to 4 s of simulation time. This is because of the mixing of intermixing of the dispersed and continuous phase, formulation of bubbles, and movement of the bubbles in an upward direction. After the 4 s, when the flow stabilizes and starts repeating a definite particulate pattern, then the curve of bed pressure drop becomes flatter. It also has been noticed for higher particle diameter.

Variation of bed pressure drop (P1–P3 and P1–P2) for a range of superficial gas velocity (0–1 m/s) at a particular size of particles (0.280 mm) has been depicted in Fig. 6. It can be noticed from Fig. 6 that the value of bed pressure drop increases up to superficial gas velocity (0.184 m/s) and, after that, attain a constant value. This is because solid particles are in contact with each other at the initial stage of fluidization and have more cohesive force between the particles, so more pressure drag is required to break this interparticle cohesive force. Once the interparticle force breaks, there is no further increment in the bed pressure drop with an increase in the superficial gas velocity. It also has been concluded that with the increase in the superficial gas velocity, the pressure drop in the upper half of the bed increases more rapidly compared to the lower half of the bed. This is because there will be a more solid volume fraction at a higher velocity at the upper half of the bed than the lower half, so there will be more pressure drop. Variation of void fraction along the height of the riser for three different diameters of the particles (0.180, 0.280 and 0.380 mm) at a constant superficial gas velocity ($3U_{mf}$) has been depicted in Fig. 7. It can be observed from the graph that the void fraction curve shows an up and down trend up to a particular height inside the riser. This is due to the bubble formation and intermixing of the phases at the lower section of the riser. After that void fraction rises and attains a constant value of 1, which indicates that there are no solid particles above that height inside the riser section, by comparing the void fraction graph for different diameters of particles (0.180, 0.280 and 0.380 mm) conclusion can be made that for smaller diameter of particles there is more void fraction has been observed in the lower section of the riser. Figure 8 shows the variation of void fraction along with the height of the riser for different superficial gas velocities ($3U_{mf}$, $4U_{mf}$ and $5U_{mf}$)

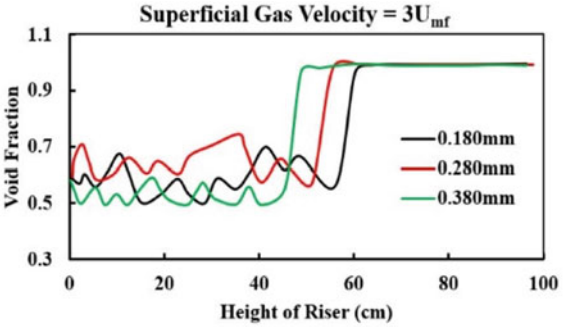

Fig. 7 Variation of void fraction along the height of riser for different particles size

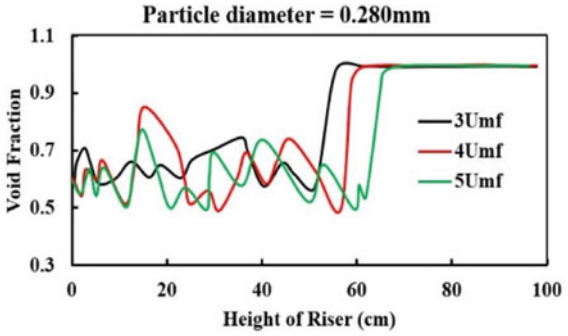

Fig. 8 Variation of void fraction along with the height of riser for different superficial gas velocity

$_{at}$ a constant (0.280 mm) diameter of particles. From the graph, it can be noticed that void fraction curves show the up and down jump in the bottom section of the riser. This is due to the fact of intermixing and high turbulence inside the system. It can also be concluded that at higher superficial gas velocity, the void fraction curve reaches a value at a higher height. This is because dispersed phase particles get lifted to a higher height at a high superficial gas velocity. Figure 9 shows the variation of void fraction for three different diameters of particles (0.180, 0.280 and 0.380 mm) at $3U_{mf}$ superficial gas velocity along the width of the riser.

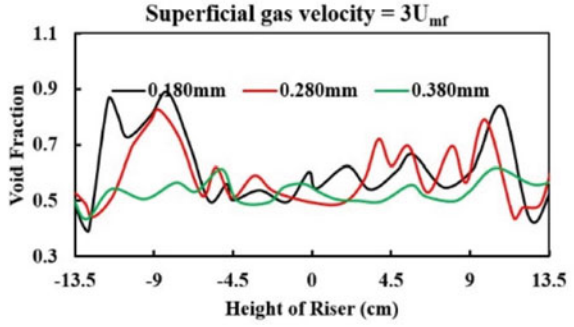

Fig. 9 Variation of void fraction along the width of riser for different particles size

8 Solid Volume Fraction Contours

Contours of volume fraction for dispersed phase at different time intervals are shown in figure below. At time $t = 0$ s, all solid particles are at rest at the base of the riser; as air enters with the proceeding of time inside the riser section through the distributor plate, it applies the drag force over the particles. As a result of drag force, the bunch of particles start lifting inside the riser, lift to 0.4 s and then fall towards the base plate. Upon this, air bubble formation starts inside the riser and creates high turbulence by mixing the phases. These bubbles form at various locations in the riser, and as time proceeds, at the top surface of the fluidized bed, these bubbles blend and expand in size and rapture. The same phenomenon of lifting a bunch of particles, bubble formation and intermixing of the particles has also been observed in sawdust simulation.

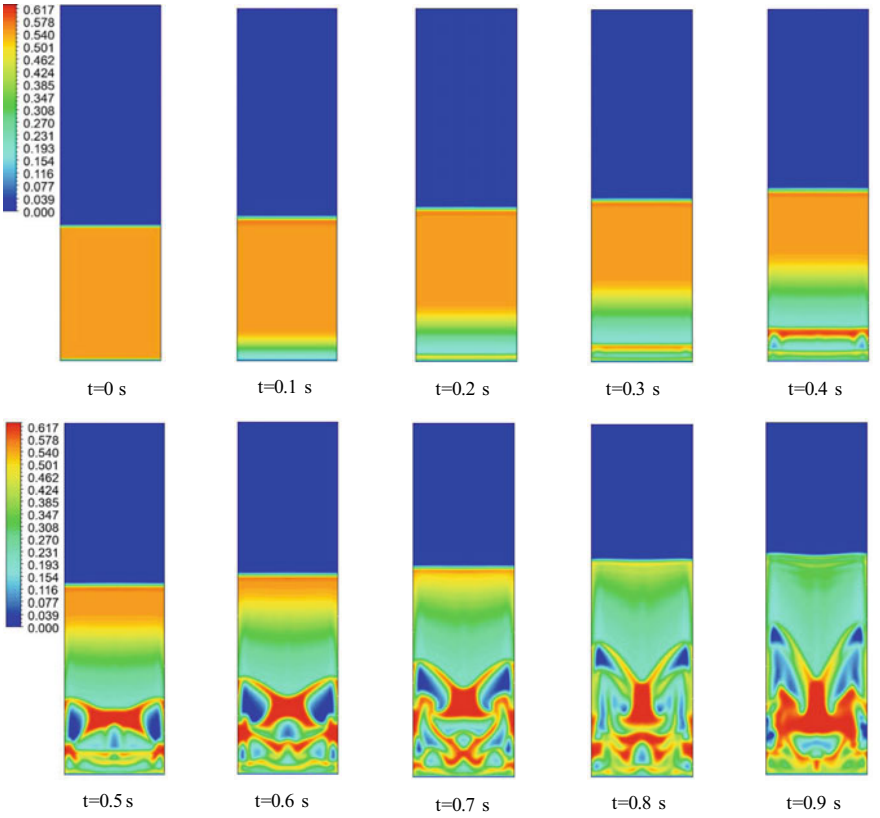

9 Conclusions

To better design of fluidized bed boiler, a detailed hydrodynamics study is required. This hydrodynamic study will guide us for better gasification and combustion inside the fluidized bed boiler. The outcome from the detailed study is presented below:

- Using the Eulerian–Eulerian two-fluid process, hydrodynamics analysis of three distinct Geldart B groups of particles (0.180, 0.280 and 0.380 mm) was conducted within a 2D riser.
- Fluidized bed pressure drops increased as particle diameter increased; a maximum value of 7 kPa was observed with particle diameter 0.380 mm, and a minimum value of 5.5 kPa was observed with a particle diameter of 0.180 mm. With a particle diameter of 0.280 mm, a pressure drop of 6 kPa was observed.
- Based on the simulation results, the value of bed pressure drop increases as the superficial gas velocity increases up to the minimum fluidization velocity (0.184 m/s), beyond which there is no additional rise in bed pressure drop as the superficial gas velocity increases.
- By examining the void fraction curve along with the riser's height, it can be inferred that bubble forming and high phase intermixing occurred in the lower portion of the riser, which is beneficial for heat and mass transfer within the fluidized bed riser. The fluidized bed's height rises as particle diameter decreases. With 0.180 mm particle diameter, the fluidized bed height increased to 60 cm, while with 0.380 mm particle diameter, the fluidized bed height decreased to 45 cm.
- Furthermore, it has been observed that as the superficial gas velocity increases, the fluidized bed height increases. At 0.280 mm particle diameter, the highest fluidized bed height (65 cm) was observed at five times minimum fluidization velocity ($5U_{mf}$). In contrast, the lowest fluidized bed height (50 cm) was observed at three times minimum fluidization velocity ($3U_{mf}$).

References

1. Hai Z, Xiuqing X (2004) Particulate concentration enrichment of primary air in pulverized coal boilers. China Particuol 2:230–233
2. Weinstein W, Graff RA, Meller M, Shao MJ (1983) The effect of the imposed pressure drop across a fast fluidized bed. In: Kunii D, Toei R (eds) Fluidization, engineering foundation. United Engineering Trustees, Inc., New York, pp 299–306
3. Ebert TA, Glicksman LR, Lints M (1993) Determination of particle and gas convective heat transfer component in circulating fluidized bed. Chem Eng Sci 48:2179–2188
4. Mahapatro A, Kalita P, Mahanta M, Saha UK, Mallick SS (2014) Numerical simulation of gas-solid flow in a pressurized circulating fluidized bed riser. In: Proceedings of the 11th international conference on fluidized bed technology, vol 11, pp 323–328
5. Kalita P, Saha UK, Mahanta P (2013) Parametric study on the hydrodynamics and heat transfer along the riser of a pressurized circulating fluidized bed unit. Exp Thermal Fluid Sci 44:620–630

6. Tymoteusz S, Renata K, Anna B, Wojciech M, Tomasz C, Aleksander P (2020) Advanced approach to modelling of pulverized coal boilers for SNCR process optimization-review and recommendations. Int J Thermofluid 224: 472–478
7. Rezwanul K, Jamal N (2017) Numerical modelling of solid biomass combustion: difficulties in initiating the fixed bed combustion. Energy Proc 110:390–395
8. Kunii D, Levenspiel O (1991) Fluidization engineering, 2nd edn. Butterworth-Heinemann, Boston, MA, USA
9. Souza-Santos ML (2004) Solid fuels combustion and gasification. CRC Press, pp 1–431. ISBN-13: 978-1420047493
10. Ergun S, Orning AA (1949) Fluid flow through randomly packed columns and fluidized beds. Ind Eng Chem 41(6):1179–1184
11. Gupta AVSSKS, Nag PK (2002) Bed-to-wall heat transfer behaviour in a pressurized circulating fluidized bed. Int J Heat Mass Transf 45(16):3429–3436
12. Casleton DK, Shadle LJ, Ross AA (2010) Measuring the voidage of a CFB through image analysis. Powder Technol 203(1):12–22
13. Mahmoudi S, Baeyens J, Seville J (2011) The solids flow in the CFB-riser quantified by single radioactive particle tracking. Powder Technol 211(1):135–143
14. Sagegh S, Peter T, Edward J, Robin W, Ping L (2018) Scale up challenges and opportunities for carbon capture by oxy-fuel circulating fluidized beds. Appl Energy 232:527–542
15. Ravelli S, Perdichizzi A, Barigozzi G (2008) Description application and numerical modelling of bubbling fluidized bed combustion in waste to energy plant. Prog Energy Combust Sci 34:224–253
16. Zhao Y, Tang L, Luo Z, Liang C, Xing H, Wu W, Duan C (2010) Experimental and numerical simulation studies of the fluidization characteristics of a separating gas–solid fluidized bed. Fuel Process Technol 91:1819–1825